Journal of Medicinal Chemistry Article

J. Med. Chem. **2010,** *53,* 7767–7777 **7767**
DOI: 10.1021/jm100729b

Synthesis and Biological Analysis of Prostate-Specific Membrane Antigen-Targeted Anticancer Prodrugs

Sumith A. Kularatne,[†] Chelvam Venkatesh,[†] Hari-Krishna R. Santhapuram,[‡] Kevin Wang,[‡] Balasubramanian Vaitilingam,[†] Walter A. Henne,[†] and Philip S. Low*[,†]

[†]*Department of Chemistry, Purdue University, 560 Oval Drive, West Lafayette, Indiana 47907, United States, and* [‡]*Endocyte, Inc., 3000 Kent Avenue, West Lafayette, Indiana 47906, United States*

Received June 16, 2010

Ligand-targeted therapeutics have increased in prominence because of their potential for improved potency and reduced toxicity. However, with the advent of personalized medicine, a need for greater versatility in ligand-targeted drug design has emerged, where each tumor-targeting ligand should be capable of delivering a variety of therapeutic agents to the same tumor, each therapeutic agent being selected for its activity on a specific patient's cancer. In this report, we describe the use of a prostate-specific membrane antigen (PSMA)-targeting ligand to deliver multiple unrelated cytotoxic drugs to human prostate cancer (LNCaP) cells. We demonstrate that the PSMA-specific ligand, 2-[3-(1, 3-dicarboxy propyl)ureido] pentanedioic acid, is capable of mediating the targeted killing of LNCaP cells with many different therapeutic warheads. These results suggest that flexibility can be designed into ligand-targeted therapeutics, enabling adaptation of a single targeting ligand for the treatment of patients with different sensitivities to different chemotherapies.

Introduction

Most cancer therapies today involve treatment with cytotoxic drugs that distribute indiscriminately into virtually all cells of the body and cause damage to malignant and healthy cells alike. Because such conventional chemotherapies are primarily designed to kill rapidly dividing cells, they also destroy proliferating healthy cells, leading to off-target toxicities that can include myelosuppression, mucositis, alopecia, nausea/vomiting, anemia, peripheral neuropathy, fatigue, etc.[1−6] Clearly, cytotoxic therapies that can be targeted selectively to pathologic cells, avoiding collateral damage to healthy cells, would constitute a significant advance in the treatment of cancer.

Two major classes of targeted therapies are currently under clinical development. First, chemotherapeutic agents are being designed to target novel functionalities or processes that emerge primarily during pathogenesis and are critical for proliferation and/or survival of the pathologic cell but are not important for the function or survival of normal cells. A prominent example of this class of targeted therapeutics is imatinib mesylate, a tyrosine kinase inhibitor that is designed to block *bcr-abl* (breakpoint cluster region-abelson), a proto-oncogene product formed by chromosomal translocation only in chronic myelogenous leukemia (CML)[a] cells.[7] Another example of a functionality-targeted therapeutic agent is bevacizumab, which suppresses growth of new blood vessels required for tumor proliferation, but has little impact on the maintenance or survival of the vasculature healthy tissues.[8−11]

A second major class of targeted therapies involves the use of tumor-specific ligands to deliver an attached nonselective cancer drug specifically to malignant cells.[12−15] When such a homing ligand exhibits strong specificity for a cancer cell, the derived ligand-targeted therapies can yield high tumor response rates with low toxicity to normal tissues. Moreover, if the chemotherapeutic agent is released only after uptake and trafficking deep into the target cell, efflux of the drug by multidrug resistance pumps can be greatly reduced.[16] Ligands that have been exploited for chemotherapeutic agent targeting include both monoclonal antibodies[17−20] and low molecular weight receptor-binding ligands such as peptide hormones,[21,22] receptor antagonists and agonists,[23] aptamers,[24] oligosaccharides,[25,26] oligopeptides,[27] and vitamins.[15,28]

In an effort to expand the arsenal of tumor-targeting ligands, we have synthesized a molecule termed 2-[3-(1,3-dicarboxy propyl)ureido] pentanedioic acid (DUPA)[29] that selectively binds to a cell surface glycoprotein termed prostate-specific membrane antigen (PSMA) and enters PSMA-expressing cells by PSMA endocytosis.[29−32] Because PSMA is expressed on both prostate cancer (PCa) cells and the neovasculature of other solid tumors but is largely absent from healthy tissues, it constitutes an ideal cell surface protein for tumor-specific targeting.[30,33] In a recent effort to evaluate the specificity of DUPA conjugates for prostate cancers, we have examined the uptake of a DUPA-targeted ^{99m}Tc radioimaging agent by human lymph node prostate cancer (LNCaP) tumors in

*To whom correspondence should be addressed. Tel: 765-494-5273. Fax: 765-494-5272. E-mail: plow@purdue.edu.

[a] Abbreviations: PSMA, prostate-specific membrane antigen; LNCaP, lymph node prostate cancer; PCa, prostate cancer; CML, chronic myelogenous leukemia; DUPA, 2-[3-(1,3-dicarboxy propyl)ureido] pentanedioic acid; PMPA, 2-(phosphonomethyl)pentanedioic acid; GSH, glutathione; DTT, dithiothreitol; HOBt, *N*-hydroxybenzotriazole; HBTU, *O*-benzotriazole-*N*,*N*,*N*′,*N*′-tetramethyl-uronium-hexafluoro-phosphate; SPPS, solid-phase peptide synthesis; RP-HPLC, reverse-phase high-performance liquid chromatography; UPLC, ultra high-pressure liquid chromatography; DidB, didemnin B; Cpt, camptothecin; VrcA, verrucarin A; PTax, paclitaxel; DAVB, desacetylvinblastine; DAVBH, desacetylvinblastine hydrazide; Tub, tubulysin B; TubH, tubulysin B hydrazide; Dox, doxorubicin.

Published on Web 10/11/2010

athymic nude mice and found retention of the agent limited to the PCa xenograft and the kidneys.[29] Because human kidneys, unlike murine kidneys,[34] express only low levels of PSMA,[30] we hypothesized that DUPA might constitute an ideal ligand for a PCa-targeted therapy. In this paper, we describe the synthesis, structure validation, and biological properties of a series of PSMA-targeted disulfide-bridged self-immolative chemotherapeutic agents and identify several targeted prodrugs that warrant consideration for clinical development.

Experimental Section

Materials. Amino acids were purchased from Chem-Impex Int (Chicago, IL). *N*-Hydroxybenzotriazole (HOBt) and *O*-benzotriazole-*N*,*N*,*N*′,*N*′-tetramethyl-uronium-hexafluoro-phosphate (HBTU) were obtained from Peptide Int. (Louisville, KY). 2-(Phosphonomethyl)pentanedioic acid (PMPA) was purchased from Axxora Platform (San Diego, CA). Tubulysin B (Tub) and desacetylvinblastine (DAVB) were provided by Endocyte Inc. (West Lafayette, IN). Camptothecin (Cpt) was obtained from the NCI (Rockville, MD). Verrucarin A (VrcA) and didemnin B (DidB) were purchased from Sigma-Aldrich (St. Louis, MO). All other chemicals, cell culture materials, and animal feed were obtained from major suppliers.

General Methods. Moisture- and oxygen-sensitive reactions were carried out under an argon atmosphere. Solid-phase peptide synthesis (SPPS) was performed using a standard peptide synthesis apparatus (Chemglass, Vineland, NJ). Flash chromatography was conducted with silica gel as the solid phase, and thin-layer chromatography (TLC) was performed on silica gel TLC plates (60 f254, 5 cm × 10 cm) and visualized under UV light. All peptides and peptide conjugates were purified by preparative reverse-phase high-performance liquid chromatography (RP-HPLC; Waters, xTerra C18 10 μm; 19 mm × 250 mm) and analyzed by analytical RP-HPLC (Waters, X-Bridge C_{18} 5 μm; 3.0 mm × 50 mm) or ultra high-pressure liquid chromatography (UPLC) (Acquity, BEH C_{18} 1.7 μm; 2.1 mm × 50 mm). ^{1}H spectra were acquired with a Bruker 400 or 500 MHz NMR spectrometer equipped with a TXI cryoprobe. Samples were run in 5 mm NMR tubes using $CDCl_3$, DMSO-d_6, or DMSO-d_6/D_2O. Presaturation was used to reduce the intensity of the residual H_2O peak. All ^{1}H signals are recorded in ppm with reference to residual $CHCl_3$ (7.27 ppm) or DMSO (2.50 ppm), and data are reported as s = singlet, d = doublet, t = triplet, q = quartet, m = multiplet or unresolved, and b = broad, with coupling constants in Hz. Liquid chromatography/mass spectrometry (LC/MS) analyses were obtained using a Waters micromass ZQ 4000 mass spectrometer coupled with a UV diode array detector. High-resolution mass spectrometric results were obtained by matrix-assisted laser desorption ionization (MALDI) mass using an Applied Biosystems (Framingham, MA) Voyager DE PRO mass spectrometer. This instrument utilizes a nitrogen laser (337 nm UV laser) for ionization with a time-of-flight mass analyzer. The matrix used for these samples was α-cyano-4-hydroxy cinnamic acid, and the peptide LHRH was used as an internal standard.

Cell Culture. LNCaP cells were obtained from the American Type Culture Collection (Rockville, MD) and grown as a monolayer in 1640 RPMI medium containing 10% heat-inactivated fetal bovine serum, 1% sodium pyruvate (100 mM), and 1% penicillin streptomycin in a 5% carbon dioxide:95% air-humidified atmosphere at 37 °C.

Synthesis and Characterization. DUPA, the ligand used to target PSMA, was synthesized as previously described.[35] Peptide spacers used to attach DUPA to its therapeutic warhead were synthesized by standard fluorenylmethyloxycarbonyl (Fmoc) solid-phase peptide chemistry starting with Cys(4-methoxytrityl)-Wang resin (Scheme 2). Disulfide-activated prodrugs [tubulysin B hydrazide (TubH),[36] DAVB hydrazide,[37] and Cpt[38]] were synthesized from the commercially available drugs according to literature procedures.

Synthesis of 2-(Pyridine-2-yl-disulfanyl) Ethanol (2). To a solution of methoxycarbonylsulfenyl chloride (3.1 mL, 34.25 mmol) in CH_3CN (30.0 mL) at 0 °C, 2-mercaptoethanol (2.4 mL, 34.25 mmol) in CH_3CN (1.0 mL) was added dropwise, and the reaction mixture was allowed to stir at −10 °C for 30 min. A solution of 2-thiopyridine (3.46 g, 31.13 mmol) in CH_3CN (18.0 mL) was added to the reaction mixture and refluxed for 2 h. The reaction mixture was then stirred at 10 °C for 1 h and filtered. The solid was washed with CH_3CN and dried under vacuum at room temperature to yield the pure product as a colorless solid (4.0 g, 57.5%). ^{1}H NMR (DMSO-d_6): δ 3.06 (t, J = 6.0 Hz, 2H), 4.18 (t, J = 6.1 Hz, 2H), 7.25 (t, J = 6.0 Hz, 1H), 7.78 (d, J = 7.9 Hz, 1H), 7.83 (t, J = 7.5, 1H), 8.45 (d, J = 4.0 Hz, 1H). ESI/MS (m/z): $(M + H)^+$ calcd for $C_7H_{10}NOS_2$, 188.3; found, 188.0.

Synthesis of 2-[Benzotriazole-1-yl-(oxycarbonyloxy)ethyl-disulfanyl]pyridine (3). To a solution of 2-(pyridine-2-yl-disulfanyl) ethanol (2.0, 8.94 mmol), HOBT (1.58 g, 11.71 mmol), and TEA (1.25 mL, 8.94 mmol) in CH_3CN (35 mL) at 0 °C, diphosgene (0.72 mL, 5.98 mmol) was added. The reaction mixture was heated to 50 °C and stirred for 24 h. The solid was filtered, washed with CH_3CN, and dried under vacuum at room temperature to yield the pure product as a pale white solid (3.48 g, 95.7%). ^{1}H NMR (DMSO-d_6): δ 3.39 (t, J = 6.0 Hz, 2H), 4.76 (t, J = 6.0 Hz, 2H), 7.22 (m, 1H), 7.66 (t, J = 7.8 Hz, 1H), 7.78 (m, 2H), 7.92 (t, J = 7.8, 1H), 8.05 (d, J = 8.4 Hz, 1H), 8.19 (d, J = 8.4 Hz, 1H), 8.43 (d, J = 4.7 Hz, 1H). ESI/MS (m/z): $(M + H)^+$ calcd for $C_{14}H_{13}N_4O_3S_2$, 349.4; found, 349.2.

Synthesis of Hydrazinecarboxylic Acid 2-(Pyridine-2-yl-disulfanyl)-ethyl ester (4). To a solution of 2-[benzotriazole-1-yl-(oxycarbonyloxy)ethyldisulfanyl]pyridine hydrochloride (685 mg, 1.62 mmol) and DIPEA (600 μL, 3.4 mmol) in CH_2Cl_2 (5.0 mL) at 0 °C, hydrazine was added. The reaction mixture was allowed to stir at 0 °C for 15 and 30 min at room temperature. After the precipitate was filtered, the crude compound was purified using flash column chromatography (silica gel, 2% MeOH in CH_2Cl_2) to yield the product as colorless oil (371 mg, 93.4%). ^{1}H NMR (DMSO-d_6): 3.06 (t, J = 6.0 Hz, 2H, S-CH_2), 4.18 (t, J = 6.0 Hz, 2H), 7.26 (t, J = 7.8 Hz, 1H), 7.79 (d, J = 8.1 Hz, 1H), 7.83 (t, J = 7.8, 1H), 8.47 (d, J = 4.7 Hz, 1H). LC/MS (m/z): $(M + H)^+$ calcd for $C_8H_{12}N_3O_2S_2$, 246.0; found, 246.1.

Synthesis of Disulfide-Activated TubH (6). To a solution of Tub (30 mg, 0.036 mmol) in ethylacetate (600 μL) under argon at −15 °C, isobutyl chloroformate (4.7 μL, 0.054 mmol) and diisopropylethylamine (13.2 μL, 0.076 mmol) were added. After the solution was stirred at −15 °C for another 45 min under argon, a solution of compound **4** (13.4 mg, 0.054 mmol) in ethyl acetate (500 μL) was added. The reaction mixture was stirred at −15 °C for 15 min and then at room temperature for 45 min. The crude product was purified using a short column (2−8% methanol in dichloromethane) to obtain the activated TubH (**6**) as a colorless oil (34.4 mg, 90.5%). ^{1}H NMR (DMSO-d_6/D_2O): δ 0.65 (d, J = 6.1 Hz, 3H), 0.78 (m, 6H), 0.94 (d, J = 6.1 Hz, 3H), 1.02 (d, J = 7.0 Hz, 3H), 1.08 (m, 1H), 1.16 (m, 1H), 1.23 (s, 4H), 1.24 (s, 4H), 1.32 (q, J = 7.2 Hz, 2H), 1.43 (m, 2H), 1.49 (m, 4H), 1.59 (m, 1H), 1.67 (m, 1H), 1.79 (m, 1H), 1.82 (s, 1H), 1.89 (m, 1H), 2.09 (s, 6H), 2.11 (m, 1H), 2.21 (m, 2H), 2.35 (m, 1H), 2.69 (m, 1H), 2.80 (bd, 1H), 2.97 (bs, 1H), 3.08 (m, 3H), 4.11 (m, 2H), 4.20 (m, 2H), 4.40 (d, J = 9.3 Hz, 1H), 5.25 (d, J = 11.9 Hz, 1H), 5.71 (d, J = 11.5 Hz, 1H), 6.16 (b, 1H), 6.59 (d, J = 8.1 Hz, 2H), 6.97 (d, J = 6.6 Hz, 2H), 7.22 (m, 1H), 7.65−7.89 (m, 2H), 8.17 (s, 1H), 8.43 (bs, 1H). ESI/MS (m/z): $(M + H)^+$ calcd for $C_{50}H_{73}N_8O_{11}S_3$, 1057.4; found, 1057.0.

Characterization of DAVB Hydrazide (DAVBH, 8). ^{1}H NMR (DMSO-d_6/D_2O): δ 0.61 (m, 1H), 0.74 (t, J = 7.3 Hz, 3H), 0.79 (t, J = 7.5 Hz, 3H), 1.03 (d, J = 6.1 Hz, 1H), 1.16 (m, 2H), 1.29 (m, 2H), 1.58 (m, 2H), 1.94 (m, 1H), 2.30 (s, 3H), 2.35 (m, 1H), 2.65 (m, 1H), 2.69 (s, 3H), 2.89 (dd, J = 14.2, 5.2 Hz, 1H), 3.10 (m, 1H), 3.26 (d, J = 13.8 Hz, 1H), 3.54 (s, 3H), 3.72 (s, 3H), 3.82 (d, J = 5.9 Hz, 1H), 3.95 (d, J = 6.1 Hz, 1H), 3.97 (s, 1H), 4.05 (t, J = 14.4 Hz, 1H), 4.24 (sb, 1H), 5.57 (d, J = 10.1 Hz, 1H), 5.71

(dd, J = 11.0, 5.1 Hz, 1H), 6.20 (s, 1H), 6.44 (s, 1H), 6.92 (t, J = 7.5 Hz, 1H), 7.00 (t, J = 7.5 Hz, 1H), 7.15 (m, 1H), 7.25 (t, J = 8.4 Hz, 1H), 7.36 (d, J = 7.9 Hz, 1H), 8.33 (s, 1H), 8.82 (s, 1H), 9.32 (s, 1H). LC/MS (m/z): $(M + H)^+$ calcd for $C_{43}H_{57}N_6O_7$, 769.9; found, 769.5.

Characterization of Disulfide-Activated DAVBH (9). ^{1}H NMR (DMSO-d_6/D_2O): δ 0.64 (m, 1H), 0.76 (t, J = 7.3 Hz, 3H), 0.81 (t, J = 7.5 Hz, 3H), 1.03 (d, J = 6.1 Hz, 1H), 1.12 (s, 2H), 1.19 (m, 2H), 1.33 (m, 2H), 1.60 (m, 2), 1.78 (m, 1H), 2.38 (m, 2H), 2. 56 (bs, 1H), 2.67 (m, 1H), 2.78 (s, 3H), 2.90 (dd, J = 14.2, 5.2 Hz, 1H), 3.09 (s, 3H), 3.12 (m, 2H), 3.16 (bs, 1H), 3.21 (dd, J = 15.5, 4.1 Hz, 1H), 3.28 (d, J = 14.2 Hz, 1H), 3.42 (s, 1H), 3.56 (s, 3H), 3.74 (s, 3H), 3.82 (d, J = 6.5 Hz, 1H), 3.99 (s, 1H), 4.09 (m, 2H), 4.23 (m, 2H), 5.61 (d, J = 10.1 Hz, 1H), 5.71 (dd, J = 10.7, 5.8 Hz, 1H), 6.22 (s, 1H), 6.48 (s, 1H), 6.94 (t, J = 7.5 Hz, 1H), 7.02 (t, J = 7.5 Hz, 1H), 7.28 (d, J = 7.9 Hz, 2H), 7.39 (d, J = 8.0 Hz, 1H), 7.86 (m, 2H), 8.49 (bs, 1H), 8.66 (s, 1H), 9.20 (s, 1H), 9.32 (s, 1H), 9.45 (s, 1H). LRMS-LC/MS (m/z): $(M)^+$ calcd for $C_{51}H_{64}N_7O_9S_2$, 982.2; found, 982.5.

Characterization of Disulfide-Activated Cpt (10). ^{1}H NMR (DMSO-d_6): δ 0.92 (t, J = 7.4 Hz, 3H), 2.18 (m, 2H), 3.14 (t, J = 6.1 Hz, 2H), 4.32 (t, J = 6.0 Hz, 2H), 5.30 (s, 2H), 5.52 (d, J = 3.5 Hz, 2H), 7.09 (s, 1H), 7.15 (m, 1H), 7.70 (m, 2H), 7.77 (td, J = 7.75, 1.8 Hz, 1H), 7.85 (td, J = 8.0, 1.0 Hz, 1H), 8.13 (t, J = 8.1 Hz, 2H), 8.39 (dt, J = 4.8, 0.7 Hz, 1H), 8.69 (s, 1H), ESI/MS (m/z): $(M + H)^+$ calcd for $C_{28}H_{24}N_3O_6S_2$, 562.6; found, 562.3.

Characterization of Disulfide-Activated VrcA (11). Synthesis was performed similarly to the DUPA-didemin B conjugate (see above). ^{1}H NMR (DMSO-d_6): δ 0.73 (s, 3H), 0.88 (d, J = 6.8 Hz, 3H), 1.23 (s, 1H), 1.57 (t, J = 12.7 Hz, 1H), 1.62 (s, 3H), 1.72 (s, 1H), 1.92 (m, 2H), 2.78 (d, J = 3.9 Hz, 1H), 3.03 (d, J = 3.9 Hz, 1H), 3.16 (t, J = 6.1 Hz, 1H), 3.70 (d, J = 5.1 Hz, 1H), 3.94 (t, J = 11.7 Hz, 1H), 4.20 (d, J = 12.1 Hz, 1H), 4.35 (t, J = 6.0 Hz, 1H), 4.39 (d, J = 12.1 Hz, 1H), 4.84 (s, 1H), 5.31 (d, J = 4.7 Hz, 1H), 5.82 (m, 1H), 6.24 (d, J = 15.5 Hz, 1H), 6.32 (d, J = 11.1 Hz, 1H), 6.88 (t, J = 11.4 Hz, 1H), 7.25 (t, J = 6.0 Hz, 1H), 7.82 (m, 2H), 8.07 (s, 1H), 8.46 (d, J = 4.2 Hz, 1H). LC/MS (m/z): $(M + H)^+$ calcd for $C_{35}H_{42}NO_{11}S_2$, 716.8; found, 716.5.

Synthesis of Disulfide-Activated DidB (12). To a solution of DidB (15.0 mg, 0.013 mmol) in CH_2Cl_2 (0.33 mL) at 0 °C, 2-[benzotriazole-1-yl-(oxycarbonyloxy)ethyldisulfanyl]pyridine (18.0 mg, 0.047 mmol) and DMAP (8.0 mg, 0.067 mmol) were added. The reaction mixture was stirred for 2 h at room temperature, and the crude product was purified by column chromatography (0−4% methanol in dichloromethane) to afford the activated DidB, as a white solid (10.0 mg, 56%). ^{1}H NMR ($CDCl_3$): δ 0.84−0.96 (m, 23H), 1.15−1.28 (m, 6H), 1.32 (d, J = 6.9 Hz, 3H), 1.38 (m, 4H), 1.51 (d, J = 6.7 Hz, 3H), 1.56−1.79 (m, 7H), 1.98−2.17 (m, 6H), 2.26 (m, 1H), 2.34 (m, 1H), 2.54 (s, 3H), 2.63 (m, 1H), 3.02 (t, J = 6.8 Hz, 2H), 3.14 (s, 3H), 3.17−3.21 (m, 1H), 3.24 (s, 1H), 3.41(dd, J = 13.8, 4.2 Hz, 1H), 3.59 (d, J = 6.8 Hz, 2H), 3.70 (m, 2H), 3.79 (s, 3H), 4.06 (m, 2H), 4.22 (q, J = 6.9 Hz, 1H), 4.37 (m, 2H), 4.55 (dd, J = 5.8, 2.0 Hz, 1H), 4.60 (t, J = 7.6 Hz, 1H), 4.73 (t, J = 7.3 Hz, 1H), 4.79 (t, J = 9.7 Hz, 1H), 5.08 (q, J = 6.7 Hz, 1H), 5.18 (d, J = 3.4 Hz, 1H), 5.21−5.23 (m, 1H), 5.36 (dd, J = 11.2, 4.2 Hz, 1H), 6.84 (d, J = 8.6 Hz, 2H), 7.07 (d, J = 8.6 Hz, 1H), 7.11 (dt, J = 5.7, 2.1 Hz, 1H), 7.66−7.69 (m, 2H), 8.47 (d, J = 5.0 Hz, 1H). LC/MS (m/z): $(M)^+$ calcd for $C_{65}H_{96}N_8O_{17}S_2$, 1325.6; found, 1325.8.

Characterization of DUPA-Linker I (13a). The synthesis was performed as described elsewhere.[33] Analytical RP-HPLC: R_t = 7.8 min [A = 0.1 TFA (pH 2), and B = CH_3CN; solvent gradient: 5−80% B in 10 min]. ^{1}H NMR (DMSO-d_6): δ 0.93 (m, 2H), 1.08 (m, 5H), 1.27 (m, 5H), 1.69 (m, 2H), 1.90 (m, 2H), 1.94 (m, 2H), 2.10 (m, 2H), 2.24 (m, 2H), 2.62 (m, 2H), 2.78 (m, 4H), 2.88 (m, 1H), 2.96 (t, J = 6.8 Hz, 2H), 3.01 (m, 1H), 3.31 (dd, J = 13.9, 5.9 Hz, 1H), 3.62 (dd, J = 14.0, 5.9 Hz, 1H), 3.80 (q, J = 6.1 Hz, 1H), 4.07 (m, 1H, α-H), 4.37 (m, 1H, α-H), 4.42 (m, 2H, α-H), 4.66 (m, 1H, α-H), 7.18 (m, 10H). LC/MS (m/z): $(M + H)^+$ calcd for $C_{47}H_{66}N_9O_{17}S$, 1060.4; found, 1060.2. UV/vis: λ_{max} = 257 nm.

Characterization of DUPA-Linker II (13b). The synthesis of linker II was performed similarly to DUPA-linker I using SPPS. Analytical RP-HPLC: R_t = 2.2 min [A = 10 mM NH_4OAc (pH 7.0), and B = CH_3CN; solvent gradient: 10−80% B in 12 min]. ^{1}H NMR (DMSO-d_6): δ 1.01 (m, 2H), 1.14 (m, 2H), 1.30 (m, 3H), 1.70 (m, 3H), 1.89 (m, 2H), 1.95 (m, 2H), 2.08 (m, 2H), 2.23 (m, 2H), 2.65 (m, 2H), 2.79 − 3.00 (m, 9H), 3.06 (dd, J = 14.1, 4.8 Hz, 1H), 4.04 (m, 1H, α-H), 4.08 (m, 1H, α-H), 4.43 (m, 1H, α-H), 4.47 (m, 1H, α-H), 4.58 (m, 1H, α-H), 7.20 (m, 10H). LC/MS (m/z): $(M + H)^+$ calcd for $C_{40}H_{55}N_6O_{13}S$, 859.95; found, 859.67. UV/vis: λ_{max} = 257 nm.

Characterization of DUPA-Linker III (13c). The synthesis of linker III was performed as described for DUPA-linker I using SPPS. Analytical RP-HPLC: white solid, R_t = 8.2 min [A = 0.1 TFA (pH 2), and B = CH_3CN; solvent gradient: 1−50% B in 10 min]. ^{1}H NMR (DMSO-d_6/D_2O): δ 1.70 (m, 3H), 1.90 (m, 3H), 2.10 (m, 2H), 2.17 (m, 2H), 2.23 (m, 2H), 2.36 (q, J = 8.3 Hz, 1H), 2.59 (dd, J = 11.0, 5.7 Hz, 1H), 2.79 (m, 3H), 3.04 (dd, J = 9.8, 4.0 Hz, 1H), 4.07 (m, 2H), 4.13 (m, 1H), 4.37 (m, 1H), 4.47 (m, 2H), 7.19 (m, 5H), 7.87 (d, J = 8.1 Hz, 1H), 8.20 (d, J = 7.8 Hz, 1H). LC/MS (m/z): $(M + H)^+$ calcd for $C_{32}H_{43}N_6O_{17}S$, 815.7; found, 815.3. UV/vis: λ_{max} = 257 nm.

Synthesis of DUPA-TubH I (14). Into a solution of saturated sodium bicarbonate (2 mL) and HPLC grade water, argon was bubbled for 10 min. With continuous bubbling of argon, DUPA-linker I (9.2 mg, 0.0113 mmol) was dissolved in argon-purged HPLC grade water (2.0 mL), and the pH of the reaction mixture was increased to ca. 7 using argon-purged bicarbonate. A solution of disulfide activated-TubH **6** (12.0 mg, 0.0113 mmol) in THF (2.0 mL) was then added to the reaction mixture, and the solution was stirred for 10 min. After THF was removed under reduced pressure, DUPA-TubH I (DUPA-TubH I) was purified by preparative RP-HPLC [A = 2 mM sodium phosphate buffer (pH 7.1), and B = CH_3CN; solvent gradient: 5−80% B in 25 min], yielding the desired product (12.2 mg, yield = 61.3%). Analytical RP-HPLC: R_t = 1.8 min [A = 10 mM NH_4OAc (pH 7.0), and B = CH_3CN; solvent gradient: 10−100% B in 4 min]. ^{1}H NMR (DMSO-d_6/D_2O): δ 0.67 (d, J = 5.5 Hz, 3H), 0.81 (q, J = 7.8 Hz, 2H), 0.86 (d, J = 7.2 Hz, 3H), 0.96 (d, J = 6.2 Hz, 3H), 1.03 (m, 3H), 1.10 (m, 1H), 1.27 (bs, 6H), 1.47 (q, J = 7.3 Hz, 2H), 1.51 (m, 1H), 1.61 (m, 2H), 1.68 (m, 1H), 1.82 (m, 2H), 1.92 (m, 1H), 2.11 (s, 6H), 2.23 (m, 2H), 2.37 (m, 2H), 2.42 (t, J = 8.1 Hz, 1H), 2.71 (m, 1H), 3.00 (bs, 1H), 3.10 (m, 3H), 3.58 (bt, 2H), 4.13 (m, 2H), 4.22 (m, 2H, α-H), 4.26 (t, J = 7.0 Hz, 1H), 4.42 (t, J = 8.8 Hz, 1H), 5.28 (d, J = 12.1 Hz, 1H), 5.73 (d, J = 11.4 Hz, 1H), 6.18 (bs, 1H), 6.60 (d, J = 7.9 Hz, 2H), 6.97 (d, J = 7.9 Hz, 2H), 7.24 (m, 2H), 7.68 (m, 1H), 7.70 (m, 1H), 7.80 (m, 2H), 7.85 (m, 2H), 8.21 (s, 1H), 8.46 (s, 1H). LRMS (LC/MS) (m/z): 2007.0 $(M + H)^+$. UV/vis: λ_{max} = 254 nm. HRMS (MALDI) (m/z) calcd for $C_{92}H_{133}N_{16}O_{28}S_3$, 2005.8637 $(M + H)^+$; found, 2005.8624.

Characterization of DUPA-DAVBH (15). The synthesis of DUPA-DAVB hydrazide (DUPA-DAVBH) was performed as described for DUPA-TubH. Analytical RP-HPLC: R_t = 6.1 min [A = 10 mM NH_4OAc (pH 7.0), and B = CH_3CN; solvent gradient: 10−100% B in 14 min]. ^{1}H NMR (DMSO-d_6/D_2O): δ 0.62 (m, 1H), 0.73 (t, J = 7.3 Hz, 3H), 0.79 (t, J = 7.3 Hz, 3H), 0.86 (d, J = 7.2 Hz, 3H), 1.04 (m, 2H), 1.16 (m, 6H), 1.31 (m, 3H), 1.57−2.16 (ms, 6H), 2.25 (m, 2H), 2.36 (m, 2H), 2.50−2.70 (ms, 4H), 2.77 (bs, 3H), 2.80−3.30 (ms, 10H), 3.53 (s, 3H), 3.71 (m, 3H), 3.98 (m, 1H), 4.10 (m, 1H), 4.18 (m, 2H), 4.42 (m, 2H), 5.60 (d, J = 10.1 Hz, 1H), 5.68 (d, J = 11.0 Hz, 1H), 6.20 (s, 1H), 6.22 (s, 1H), 6.43 (s, 1H), 6.91 (t, J = 7.7 Hz, 2H), 7.00 (t, J = 7.3 Hz, 1H), 7.03 (d, J = 7.5 Hz, 1H), 7.05−7.29 (ms, 6H), 7.36 (d, J = 7.8 Hz, 1H), 7.72 (bs, 2H), 7.86 (bs, 2H), 7.93 (s, 1H), 8.02 (s, 1H), 9.16 (s, 1H), 9.34 (s, 1H). LRMS (LC/MS) (m/z): 1932.2 $(M + H)^+$. UV/vis: λ_{max} = 254 nm. HRMS (MALDI) (m/z): calcd for $C_{93}H_{124}N_{15}O_{26}S_2$, 1930.8283 $(M + H)^+$; found, 1930.8273.

Synthesis and Characterization DUPA-Cpt (16). The synthesis of DUPA-Cpt was performed as described for DUPA-TubH. Analytical RP-HPLC: R_t = 5.3 min [A = 10 mM NH_4OAc (pH 7.0),

and B = CH_3CN; solvent gradient: 10−100% B in 14 min]. ^{1}H NMR (DMSO-d_6/D_2O): δ 0.89 (t, J = 7.5 Hz, 3H), 1.00 (m, 1H), 1.11 (m, 2H), 1.28 (m, 1H), 1.67 (m, 1H), 1.78 (m, 1H), 1.85 (m, 1H), 1.98 (m, 1H), 2.07 (m, 1H), 2.14 (m, 1H), 2.23 (m, 1H), 2.84 (bt, J = 11.9 Hz, 1H), 2.94 (m, 1H), 3.31−2.99 (ms, 3H), 3.96 (m, 1H), 4.06 (q, J = 6.5 Hz, 1H), 4.17 (m, 1H), 4.27 (t, J = 5.8 Hz, 1H), 4.34 (t, J = 6.1 Hz, 1H), 4.42 (m, 1H), 4.65 (m, 1H), 5.30 (bs, 1H), 5.50 (bs, 1H), 7.10 (m, 10H), 7.71 (t, J = 7.5 Hz, 1H), 7.81 (t, J = 6.6 Hz, 1H), 7.86 (t, J = 7.7 Hz, 1H), 8.12 (d, J = 8.1 Hz, 1H), 8.19 (d, J = 8.5 Hz, 1H), 8.59 (bs, 1H), 8.69 (s, 1H), 8.98 (d, J = 7.5 Hz, 1H), 9.47 (bt, 1H). LRMS (LC/MS) (m/z): 1511.1 $(M + H)^+$. UV/vis: λ_{max} = 254 nm. HRMS (MALDI) (m/z): calcd for $C_{70}H_{84}N_{11}O_{23}S_2$, 1510.5183 $(M + H)^+$; found, 1510.5176.

Synthesis and Characterization of DUPA-VrcA (17). The synthesis of DUPA-VrcA disulfide was performed as described for DUPA-Tub. Analytical RP-HPLC: R_t = 1.4 min [A = 10 mM NH_4OAc (pH 7.0), and B = CH_3CN; solvent gradient: 10−100% B in 4 min]. ^{1}H NMR (DMSO-d_6/D_2O): δ 0.73 (s, 3H), 0.86 (d, J = 6.8 Hz, 3H), 1.05 (m, 1H), 1.15 (m, 1H), 1.23 (s, 1H), 1.33 (m, 1H), 1.55 (m, 1H), 1.63 (s, 3H), 1.72 (s, 2H), 1.88−2.08 (m, 2H), 2.78 (bd, J = 3.5 Hz, 1H), 2.97 (m, 1H), 3.01 (d, J = 2.5 Hz, 1H), 3.69 (bd, J = 4.7 Hz, 1H), 3.91 (m, 1H), 3.98 (m, 1H), 4.05 (m, 1H), 4.17 (m, 1H), 4.31 (m, 1H), 4.39 (m, 1H), 4.82 (s, 1H), 5.30 (bd, J = 4.7 Hz, 1H), 5.82 (m, 1H), 6.22 (d, J = 15.9 Hz, 1H), 6.30 (d, J = 11.5 Hz, 1H), 6.88 (t, J = 11.3 Hz, 2H), 7.21 (ms, 11H), 7.84 (t, J = 14.3 Hz, 1H). LRMS (LC/MS) (m/z): 1664.9 $(M + H)^+$. UV/vis: λ_{max} = 254 nm. HRMS (MALDI) (m/z): calcd for $C_{77}H_{102}N_9O_{28}S_2$, 1664.6276 $(M + H)^+$; found, 1664.6265.

Synthesis and Characterization of DUPA-DidB (18). The synthesis of DUPA-DidB was performed as described for DUPA-TubH. White solid, analytical RP-HPLC: R_t = 1.9 min [A = 10 mM NH_4OAc (pH 7.00, and B = CH_3CN; solvent gradient: 10−100% B in 4 min]. ^{1}H NMR (DMSO-d_6/D_2O): δ 0.73−0.95 (m, 9H), 0.99 (d, J = 5.6 Hz, 1H), 1.05 (m, 1H), 1.15 (d, J = 6.8 Hz, 3H), 1.19−1.29 (ms, 4H), 1.34 (d, J = 6.6 Hz, 3H), 1.47−2.26 (ms, 19H), 2.82 (s, 2H), 2.85−2.99 (m, 3H), 3.02 (s, 3H), 3.04−3.25 (ms, 3H), 3.35 (s, 3H), 3.47 (dd, J = 13.8, 4.2 Hz, 1H), 3.61 (m, 1H), 3.72 (s, 3H), 3.79 (m, 1H), 3.92−4.50 (ms, 15H), 4.60−5.00 (ms, 12H), 5.16 (d, J = 7.5 Hz, 1H), 5.22 (dd, J = 11.1, 4.0 Hz, 1H), 6.85 (d, J = 8.5 Hz, 4H), 7.08−7.29 (ms, 10H). LRMS (LC/MS) (m/z): $[(M + 2)/2]^{+2}$ 1138.2. UV/vis: λ_{max} = 254 nm. HRMS (MALDI) (m/z): calcd for $C_{107}H_{157}N_{16}O_{34}S_2$, 2274.0490 $(M + H)^+$; found, 2274.0657.

Synthesis and Characterization of DUPA-TubH II (19). The synthesis of DUPA-TubH (linker II) was performed as described for DUPA-Tub. Analytical RP-HPLC: R_t = 2.2 min [A = 10 mM NH_4OAc (pH 7.0), and B = CH_3CN; solvent gradient: 10−100% B in 4 min]. ^{1}H NMR (DMSO-d_6/D_2O): δ 0.66 (d, J = 6.1 Hz, 3H), 0.80 (q, J = 7.5 Hz, 5H), 0.96 (d, J = 6.3 Hz, 3H), 1.00 (d, J = 6.2 Hz, 3H), 1.14 (m, 3H), 1.27 (m, 1H), 1.32 (m, 1H), 1.47 (m, 2H), 1.54 (m, 1H), 1.61−1.68 (ms, 2H), 1.81 (m, 2H), 1.92 (m, 3H), 2.04 (s, 3H), 2.10 (s, 3H), 2.17−2.39 (ms, 8H), 2.66−2.99 (ms, 6H), 3.06 (dd, J = 13.3, 4.4 Hz, 1H), 3.34 (m, 2H), 3.87 (m, 1H), 4.00 (m, 1H), 4.06 (m, 1H), 4.20 (m, 1H), 4.24 (t, J = 7.0 Hz, 1H), 4.40 (t, J = 8.8 Hz, 1H), 4.44 (m, 1H), 5.25 (d, J = 12.1 Hz, 1H), 5.74 (d, J = 11.4 Hz, 1H), 6.22 (bs, 1H), 6.62 (d, J = 7.9 Hz, 2H), 6.99 (d, J = 7.9 Hz, 2H), 7.13−7.27 (m, 10H), 7.92 (m, 2H), 8.24 (s, 1H), 8.46 (s, 1H), 9.16 (s, 1H), 9.21 (s, 1H), 9.70 (s, 1H). LRMS (LC/MS) (m/z): 1805.4 $(M + H)^+$. UV/vis: λ_{max} = 254 nm. HRMS (MALDI) (m/z): calcd for $C_{85}H_{122}N_{13}O_{24}S_3$, 1804.7888 $(M + H)^+$; found, 1804.7879.

Synthesis and Characterization of DUPA-TubH III (20). The synthesis of DUPA-TubH (linker III) was performed as described for DUPA-Tub. Analytical RP-HPLC: R_t = 7.3 min [A = 10 mM NH_4OAc (pH 7.0), and B = CH_3CN; solvent gradient: 1−50% B in 10 min]. ^{1}H NMR (DMSO-d_6/D_2O): δ 0.59 (d, J = 5.5 Hz, 3H), 0.65 (t, J = 7.3 Hz, 3H), 0.72 (t, J = 7.3 Hz, 3H), 0.76 (d, J = 6.4 Hz, 3H), 0.86 (m, 1H), 0.90 (d, J = 6.0 Hz, 3H), 1.00 (d, J = 6.7 Hz, 3H), 1.08 (m, 2H), 1.15 (b, 3H), 1.34 (m, 7H), 1.41 (m, 3H), 1.49 (b, 1H), 1.58 (m, 5H), 1.68 (m, 2H), 1.81 (m, 7H), 1.93 (m, 2H), 1.98 (s, 3H), 2.11 (m, 2H), 2.18 (m, 2H), 2.20 (m, 2H), 2.34 (m, 3H), 2.62 (m, 1H), 2.75 (m, 3H), 2.89 (m, 2H), 3.06 (d, J = 10.9 Hz, 1H), 3.12 (d, J = 11.1 Hz, 1H), 3.76 (t, J = 6.2 Hz, 1H), 3.81 (t, J = 6.2 Hz, 2H), 3.90 (t, J = 6.4 Hz, 1H), 4.04 (b, 1H), 4.21 (b, 2H), 4.34 (m, 1H), 4.37 (m, 1H), 4.49 (m, 2H), 5.20 (d, J = 11.5 Hz, 1H), 5.65 (d, J = 11.4 Hz, 1H), 6.15 (b, 1H), 6.57 (d, J = 8.0 Hz, 2H), 6.96 (d, J = 7.4 Hz, 2H), 7.13 (d, J = 6.7 Hz, 3H), 7.18 (d, J = 6.5 Hz, 2H), 8.04 (s, 1H). LC/MS (m/z): 1758.7 $(M - H)^-$. UV/vis: λ_{max} = 254 nm. HRMS (MALDI) (m/z): calcd for $C_{77}H_{110}N_{13}O_{28}S_3$, 1758.6594 $(M - H)^-$; found, 1758.7033.

General Procedure for Relative Affinity Studies. LNCaP cells were seeded in 24-well (100000 cells/well) Falcon plates and allowed to form monolayers over a period of 48 h. The spent medium in each well was replaced with 100 nM DUPA-^{99m}Tc in the presence of increasing concentration (0.1 nM to 1 μM) of DUPA-prodrug in fresh medium (0.5 mL). After they were incubated for 1 h at 37 °C, cells were rinsed with culture medium (2 × 1.0 mL) and tris buffer (1 × 1.0 mL) to remove any unbound radioactivity. Cells were then resuspended in tris buffer (0.5 mL), and the cell-bound radioactivity was counted using a γ-counter. The relative binding affinities were calculated using a plot of % cell bound radioactivity versus the concentration of the test article using GraphPad Prism 4.

Analysis of Efficiency of Drug Release Following Disulfide Reduction. A solution of test article in phosphate buffer (1 mM, pH 7.4) was treated with a 10-fold molar excess of either glutathione (GSH) or dithiothreitol (DTT) and incubated for different lengths of time at 37 °C. The efficiency of active drug release from the intact DUPA prodrugs was monitored at λ = 254 nm by analytical RP-HPLC and LC/MS as a function of time.

General Procedure for Dose Dependence Studies. LNCaP cells were seeded in 24-well (50000 cells/well) Falcon plates and allowed to form monolayers over a period of 48 h. The old medium was then replaced with fresh medium (0.5 mL) containing increasing concentrations of drug (either targeted or nontargeted) in the presence or absence of excess PMPA (to block all accessible PSMA sites), and cells were incubated for an additional 2 h at 37 °C. Cells were washed 3× with fresh medium and incubated in fresh medium (0.5 mL) for another 66 h at 37 °C. The spent medium in each well was replaced with fresh medium (0.5 mL) containing [^{3}H]-thymidine (1 mCi/mL), and the cells were incubated for additional 4 h at 37 °C to allow [^{3}H]-thymidine incorporation. The cells were then rinsed with medium (2 × 0.5 mL) and treated with 5% trichloroacetic acid (0.5 mL) for 10 min at room temperature. After the trichloroacetic acid was replaced with 0.25 N NaOH (0.5 mL), cells were transferred to individual scintillation vials containing Ecolume scintillation cocktail (3.0 mL) and counted in a liquid scintillation analyzer. IC_{50} values were calculated by plotting %[^{3}H]-thymidine incorporation versus log concentration of DUPA-drug conjugate using in GraphPad Prism 4.

Results

Screening of Base Drugs. Because PSMA is expressed at only ~10^6 copies/PCa cell, it was reasoned that only highly potent chemotherapeutic agents could be targeted in sufficient quantities to kill PCa cells in vivo. In an effort to identify chemotherapeutic agents with the required potency, human PCa (LNCaP cell line) cells were pulsed for 2 h with increasing concentrations of nontargeted cytotoxic agent (see the structures in the Supporting Information, Figure 1), washed to remove unbound drug, and chased for 66 h in fresh medium to allow each cytotoxin time to exert its effect. As shown in Table 1 and Figure 1, cytotoxic drugs such as Tub, DAVB, and their semisynthetic hydrazide analogues, as well as protein synthesis inhibitors such as VrcA and DidB, were all highly active in blocking LNCaP cell proliferation (IC_{50} < 13 nM). On the basis of past experience with folate-targeted drugs, an IC_{50} of $<10^{-8}$ M was considered sufficient to ensure efficacy

Table 1. Effect of Various Nontargeted Cytotoxic Drugs on the Survival of LNCaP Cells in Culture

drug	class	IC_{50} (nM)	clog P^a
PTax	taxanes	22.3	4.40
DAVB	vinca alkaloids	9.5	2.89
DAVBH	vinca alkaloids	12.2	0.73
Tub	vinca alkaloids	2.5	7.20
TubH	vinca alkaloids	3.7	6.05
Cpt	topo-isomerase I	none[b]	0.89
Dox	topo-isomerase II	77.6	0.32
VrcA	protein synthesis inhibitors	3.3	−1.93
DidB	protein synthesis inhibitors	2.8	6.34
cis-platin	DNA alkylating agent	none[b]	−2.83
prednisolone	anti-inflammatory agent	none[b]	1.42
RWJ67657	P38 MAP kinase inhibitor	none[b]	4.14
SB203580	P38 MAP kinase inhibitor	none[b]	2.99
wortmannin	PI3 kinase inhibitor	none[b]	0.21
nigericin	antibiotic/antiporter of H^+ and K^+	none[b]	2.45
paraquat	electron acceptor	none[b]	−8.65
atractyloside	inhibit oxidative phosphorylation	none[b]	1.38

[a] clog P = calculated log (partition coefficient). [b] None, not active within the 100 pM to 1 μM range.

for most ligand-targeted therapeutic agents,[40] and consequently, the above drugs were examined further for their killing potencies as DUPA-targeted conjugates.

Synthesis of PSMA-Targeted Disulfide-Bridged Self-Immolative DUPA Prodrugs. Syntheses of activated mixed disulfide forms of TubH (**6**) and desacetylvinblastine hydrazide (DAVBH) (**9**) are shown in Scheme 1. β-Mercaptoethanol (**1**) was first reacted with methoxycarbonylsulfenyl chloride and 2-thiopyridine to generate 2-(pyridine-2-yl-disulfanyl) ethanol (**2**) in quantitative yield. Compound **2** was then treated with diphosgene to form a chloroformate intermediate, followed by HOBT to furnish compound **3**. This HOBT-activated analogue **3** was transformed into the heterobifunctional linker **4** by reacting with hydrazine in dichloromethane. The carboxylic acid moiety in Tub was then activated with isobutylchloroformate and reacted with the heterobifunctional linker **4** to generate an activated mixed disulfide derivative of TubH (**6**). In the case of the activated mixed disulfide of DAVBH (**8**), vinblastine was first reacted with hydrazine in methanol followed by transformation into the activated mixed disulfide derivative of DAVBH (**9**) using HOBT analogue **3**, as shown in Scheme 1. Along similar lines, activated mixed disulfide derivatives of DidB (**12**), Cpt (**10**), and VrcA (**11**) were synthesized using their HOBT analogues **3** (Figure 2).

Design of the optimal spacer linking the aforementioned drugs to DUPA required selection of substituents that would not only improve binding affinity but also enhance overall water solubility and avoid nonspecific uptake by scavenger receptors in the liver. Because earlier studies with DUPA-targeted radioimaging agents revealed that optimal binding occurred when the spacer contained two phenylalanine residues at appropriate distances from DUPA,[35] a similar design was incorporated into construction of each of the therapeutic conjugates. To improve water solubility, several acidic groups were added toward the C terminus of the spacer and compared for optimal binding. Synthesis of these optimized DUPA-peptide spacers (**13a**−**c**) bearing a COOH-terminal cysteine was accomplished by standard fluorenylmethyloxycarbonyl (Fmoc) SPPS starting from the Fmoc-Cys(Trityl)-Wang resin, as shown in Scheme 2.

The activated mixed disulfide-bridged derivative of TubH was exchanged with the DUPA-spacer-Cys I (**13**) in water at neutral pH under argon to produce the desired PSMA-targeted disulfide-bridged self-immolative prodrug, DUPA-TubH I **14** (Scheme 3). Compounds **15**−**18** (Figure 3) were synthesized by analogous methods. Three closely related DUPA-TubH conjugates **14**, **19**, and **20** (Figure 3) were also prepared by varying the length and chemistry of the spacer to evaluate the contribution of the spacer to the solubility and specificity of the final drug conjugate.

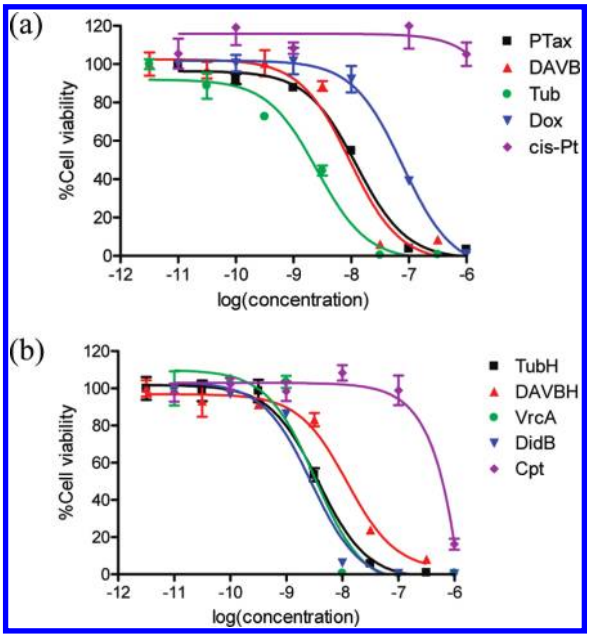

Figure 1. Effect of the drug concentration on the survival of a human PCa cell line. Free drugs dissolved in DMSO were added at the indicated concentrations to LNCaP cells in RPMI culture media and allowed to incubate for 2 h at 37 °C. Media were then removed and replaced with fresh media (drug-free), and incubation was continued for an additional 66 h. Cell survival was then quantitated using a ^{3}H-thymidine assay, as described in the General Methods. PTax, paclitaxel; Dox, doxorubicin; cis-Pt, cis-platin; DAVBH, desacetylvinblastine hydrazide. Error bars represent SD (n = 3).

Analysis of the Affinity of DUPA-Prodrug Conjugates for PSMA and Evaluation of Base Drug Release following Disulfide Reduction. The affinity of each DUPA-prodrug conjugate for PSMA was estimated by measuring the concentration of DUPA-prodrug required to block 50% binding of DUPA-^{99m}Tc to LNCaP cells. For this purpose, LNCaP cells were incubated in the presence of 100 nM DUPA-^{99m}Tc plus increasing concentrations (0.1 nM to 1 μM) of DUPA-prodrug (e.g., DUPA-TubH). Following three washes in saline to remove unbound DUPA conjugate, cells were counted for bound radioactivity. On the basis of an absolute affinity of DUPA-^{99m}Tc for PSMA of K_d = 14 nM,[29] the dissociation constant of DUPA-TubH I (**14**) for PSMA was calculated at 26 nM (Figure 4). The measured affinities of the other DUPA-prodrug conjugates range from 7 to 70 nM.

The efficiency of base drug release from its respective DUPA-prodrug conjugate was next assessed by treating each conjugate with either GSH or DTT to reduce the mixed disulfide, followed by analysis of products by analytical RP-HPLC and LC/MS. HPLC chromatograms (e.g., see Figure 5a) indicated that over 98% of disulfide bonds were reduced within 2−4 h upon addition of 10-fold excess GSH. To establish the mechanism of active drug release, selected samples were also analyzed by LC/MS at different time intervals (Figure 5b). In the case of DUPA-TubH III, as shown in Scheme 4, reduction

Scheme 1[a]

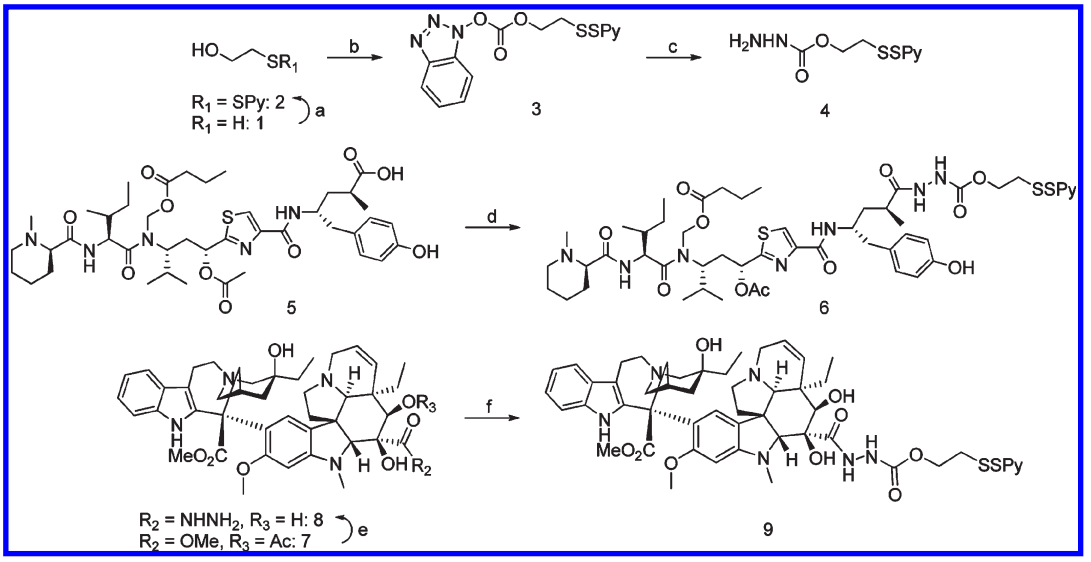

[a] Reagents and conditions: (a) (i) $MeOC(O)SCl/CH_3CN$, 0 °C, 0.5 h; (ii) 2,2′-dipyridyl-disulfide/CH_3CN, 0 °C, 2 h. (b) (i) Diphosgene, HOBt, TEA/CH_3CN, 0 °C; (ii) Δ/50 °C, 24 h. (c) NH_2NH_2, DIPEA/CH_2Cl_2, 0 °C to room temperature, 45 min. (d) (i) Isobutylchlorofomate, DIPEA/EtOAc, −15 °C, 45 min; (ii) **4**/ EtOAc, −15 °C to room temperature, 45 min. (e) NH_2NH_2/MeOH, 60 °C, 12 h. (f) Compound **3**, DIPEA/CH_2Cl_2, room temperature, 1 h. Py = pyridyl.

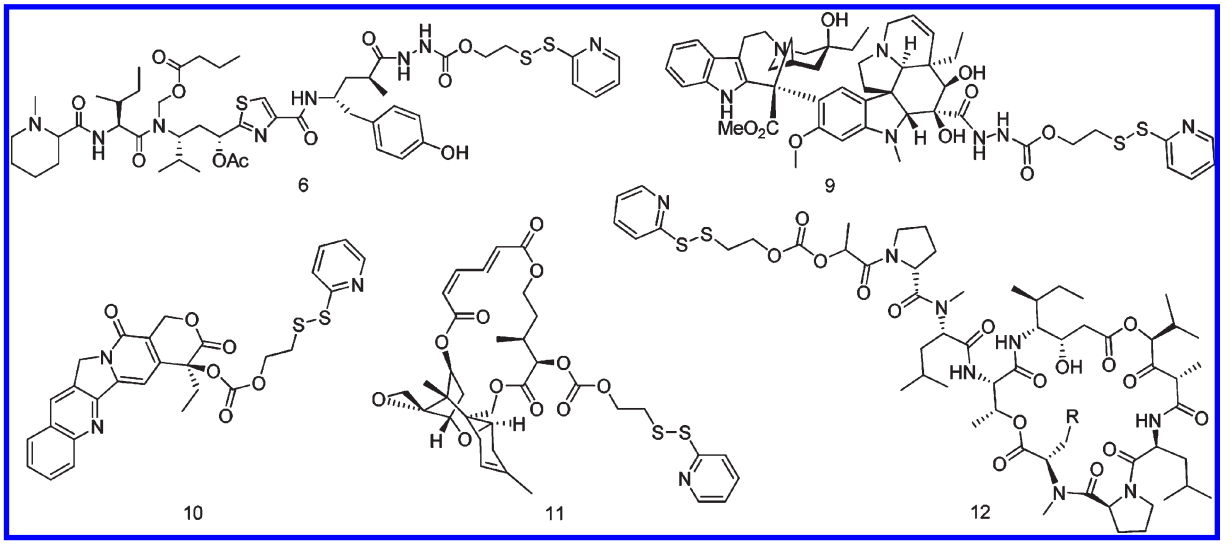

Figure 2. Structures of activated mixed disulfide-bridged cytotoxic agents. TubH (**6**), TubH; DAVBH (**9**), DAVBH; Cpt (**10**), Cpt; VrcA (**11**), VrcA; and DidB (**12**), DidB (R = *p*-methoxyphenyl).

of the disulfide bond by DTT generated a thiol intermediate that would eventually be expected to release unmodified tubulysin hydrazide via either path A or path B (Scheme 4). On the basis of LC/MS analysis, over 95% of the disulfide bonds were found to form free TubH via the carbonate intermediate **21** (Figure 5b), suggesting that efficient drug release occurs primarily via path A. Efficient release of unmodified drug upon exposure to GSH was encouraging, since it suggested that liberation of unmodified TubH should proceed spontaneously following disulfide bond reduction within the endosomes of PCa cells. Importantly, previously published in vivo studies[29] using the DUPA-tubulysin III (**20**) conjugate have demonstrated that the conjugate is sufficiently stable in circulation to reach its receptor on LNCaP tumors in its intact nonreduced form.

Cytotoxicity of DUPA-Prodrug Conjugates. Analysis of the cytotoxicity of each PSMA-targeted prodrug was then conducted by exposing LNCaP cells to the DUPA-prodrug conjugate for 2 h, followed by restoration of the cells to drug-free media for 66 h and then analysis of cell viability by quantitation of ^{3}H-thymidine incorporation. As shown in Figure 6a, ^{3}H-thymidine incorporation dramatically decreased with increasing concentrations of DUPA-TubH I−III and DUPA-DAVBH. Indeed, all DUPA-prodrug conjugates with the exception of DUPA-VrcA (**17**) showed high cytotoxicity for LNCaP cells, with IC_{50} values in the low nanomolar range. Most importantly, the high efficacy of all PSMA-targeted prodrugs was quantitatively inhibited by competition with 100-fold excess PMPA (Figure 6b), suggesting that cell killing required the presence of an empty PSMA receptor and did not occur by extracellular release of active drug followed by passive diffusion into the cell. This result is significant, since PCa cells constitute the primary site where PSMA is exposed

and accessible in humans to parenterally administered PSMA-targeted drugs.

Discussion

We have shown here that the PSMA-targeted ligand, DUPA, can be exploited to deliver a variety of cytotoxic drugs that can kill cells that express elevated levels of PSMA. Because future advances in personalized medicine will almost certainly require different therapeutic warheads for different PCa patients, this versatility in drug delivery could prove beneficial when attempting to fit any desired therapy to any individual patient. Expression of PSMA on the neovasculature of most, if not all, solid tumors will only add to the need for an adaptable targeting ligand for multiple therapeutic needs.

Although ligand targeting shows considerable promise for improving the potency and toxicity of multiple cancer therapeutics, simple attachment of a cytotoxic drug to a tumor-specific ligand may not ensure achievement of the above properties. As noted previously,[15] the potency of any ligand-targeted drug must be high, since most receptor-mediated endocytosis pathways deliver only limited quantities of drug. The spacer that links the drug to its targeting ligand must also be relatively stable to ensure its arrival at the tumor mass intact, yet sufficiently labile to enable rapid release of the unmodified therapeutic agent following internalization into the malignant cell. Indeed, many ligand-drug conjugates have failed because free drug has been released before the targeting ligand could mediate its uptake by the target cell (personal observations). Now, as observed in this paper, the innate stability of the therapeutic drug in its ligand-targeted conjugate would also appear to impact performance of the drug conjugate. Although Cpt was relatively inactive against LNCaP cells in its nontargeted form (Table 1), the drug was still found to be highly potent as a DUPA conjugate (Table 2). We hypothesize that attachment of the DUPA-spacer to Cpt at its 20-OH may have stabilized the lactone ring against hydrolysis, as reported when other moieties have been conjugated to this same site.[38−40] Such stabilization would have then rendered the conjugate capable of surviving the 2 h incubation in culture medium without hydrolyzing to its inactive form. Conversely, failure of the DUPA-VrcA conjugate to kill LNCaP cells in culture despite its high potency in free form may have derived from the different routes of cellular entry of VrcA in its targeted and nontargeted forms. Thus, hydrolases in endosomal compartments could have cleaved either the epoxide or the lactone ring of VrcA during intracellular PSMA trafficking, whereas the free drug may have found direct access to its site of action within the cell. Taken together, it is becoming more apparent that multiple variables may require optimization before a potent cytotoxic drug can be converted into a successfully targeted therapeutic agent.

As efforts to develop ligand-targeted therapies increase, it is important to consider both their advantages and disadvantages as compared with molecular-targeted therapies. As noted above, a major advantage of ligand targeted therapies can stem from their remarkable therapeutic flexibility, since almost any potent drug can be targeted to a diseased tissue if it can be linked in a reversible manner to an appropriate targeting ligand. However, because only a few chemical functionalities allow for facile release of a covalently attached drug following uptake by the targeted cell, drugs must be selected that contain one or more of a limited number of chemical moieties (−SH, −COOH, −OH, or $-NH_2$) that can be adapted for intracellular release.[15,29,36−38] A second advantage of ligand-targeted

Scheme 2[a]

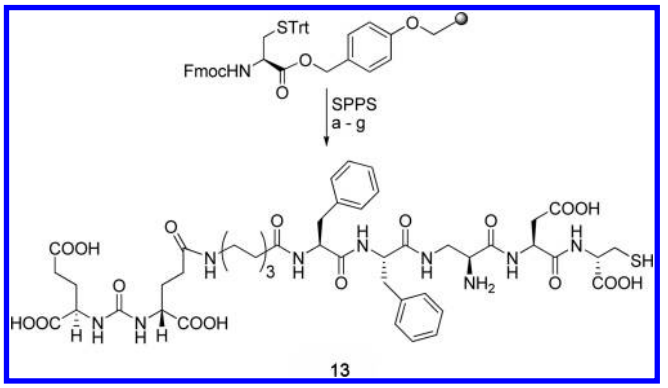

[a] Reagents and conditions: (a) (i) 20% piperidine/DMF, room temperature, 10 min; (ii) Fmoc-Asp(O^{t}Bu)-OH, HBTU, HOBt, DMF/DIPEA, 2 h. (b) (i) 20% piperidine/DMF, room temperature, 10 min; (ii) Fmoc-diaminopropionic (DAP) acid, HBTU, HOBt, DMF/DIPEA, 2 h. (c) (i) 20% piperidine/DMF, room temperature, 10 min; (ii) Fmoc-Phe-OH, HBTU, HOBt, DMF/DIPEA, 2 h. (d) (i) 20% piperidine/DMF, room temperature, 10 min; (ii) Fmoc-Phe-OH, HBTU, HOBt, DMF/DIPEA, 2 h. (e) (i) 20% piperidine/DMF, room temperature, 10 min; (ii) Fmoc-8-amino-octanoic (EAO) acid, HBTU, HOBt, DMF/DIPEA, 2 h. (f) (i) 20% piperidine/DMF, room temperature, 10 min; (O^{t}Bu)$_3$-DUPA-OH, HBTU, HOBt, DIPEA, 2 h. (g) TFA/H_2O/TIPS/EDT (92.5:2.5:2.5:2.5), 1 h.

Scheme 3[a]

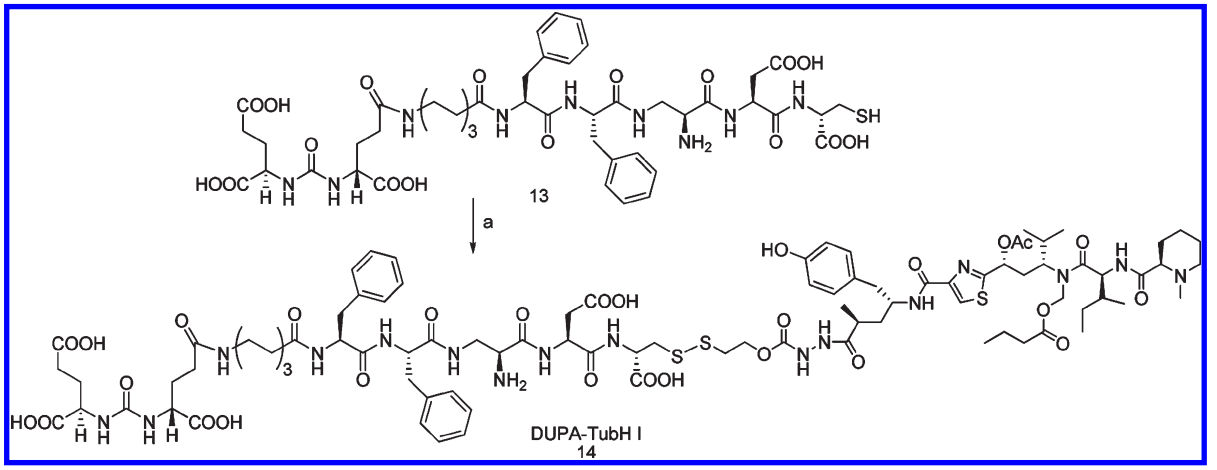

[a] Reagents and conditions: (a) (i) H_2O/$NaHCO_3$ (pH 7.0−7.2), argon, room temperature; (ii) **6**/THF, argon, room temperature, 15 min.

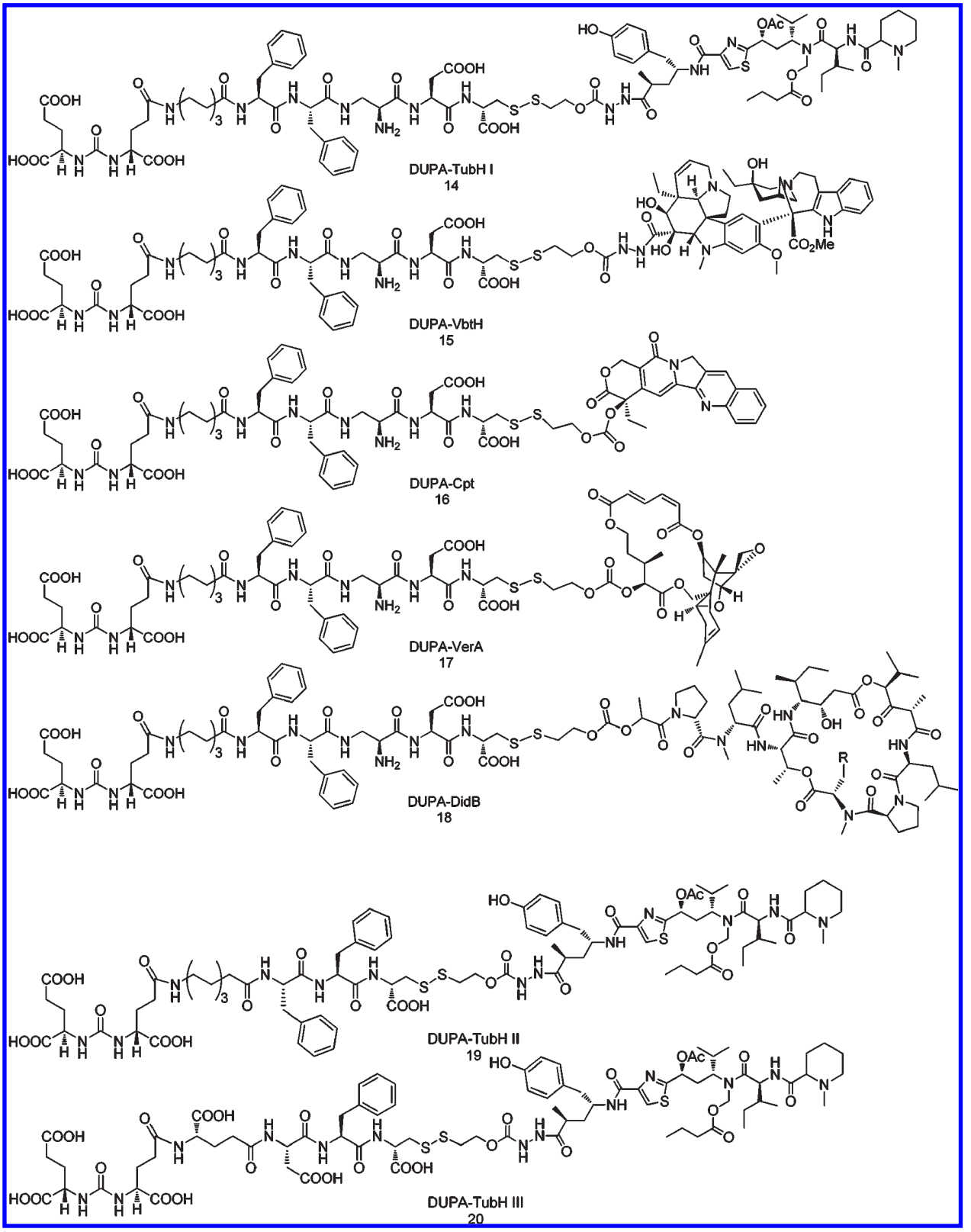

Figure 3. Structures of PSMA-targeted disulfide-bridged self-immolative prodrugs. The base drug nomenclature is as in Figure 2.

therapies derives from the ability to design a cognate imaging agent with the same targeting ligand.[15,29,35,41−43] Because such cognate imaging agents can be used to select patients for the ligand-targeted therapy and because the FDA is increasingly desirous that a diagnostic agent be employed to identify potential "responders" to any new drug, the straightforward generation of an imaging agent targeted to the same receptor renders compliance with this FDA condition relatively easy. Third, whenever membrane impermeable drugs must be delivered, ligand-targeted therapies are generally preferred, since a good targeting ligand will often carry its attached cargo into the target cell by receptor-mediated endocytosis. Thus,

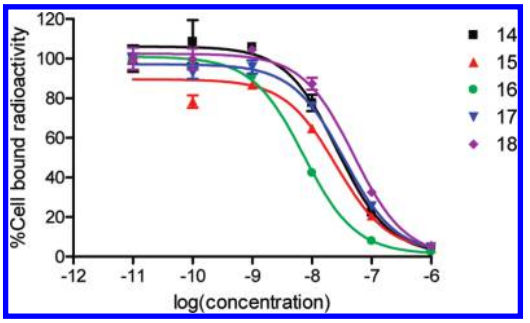

Figure 4. Relative binding affinities of DUPA-prodrugs with respect to DUPA-^{99m}Tc (a PSMA-targeted radioimaging agent). LNCaP cells were incubated for 1 h at 37 °C in the presence of 100 nM DUPA-^{99m}Tc with increasing concentrations of DUPA-prodrugs. Cell-bound radioactivity was assayed as described in the General Methods.

when proteins, dendrimers, liposomes, genes, nanoparticles, siRNA, peptides, miRNA, etc. constitute the therapeutic cargo, the use of an internalizing targeting ligand can render an otherwise inactive drug more efficacious.[43,44] Finally, because overexpression of a receptor on a pathologic cell may be more common than expression of a novel/upregulated enzyme or pathway in a pathologic cell, opportunities for development of ligand-targeted therapies may arise more frequently than opportunities for novel functionality-targeted therapies.

Ligand-targeted therapies also exhibit disadvantages relative to functionality-targeted and nontargeted therapies. First, because most endocytic pathways transport relatively few molecules into a cell, the ligand-targeted drug must be effective at very low concentrations. For some diseases, a large selection of highly potent therapeutic agents is readily available, but for other pathologies, the repertoire of potent drugs is small. Second, as noted above, an efficient drug release

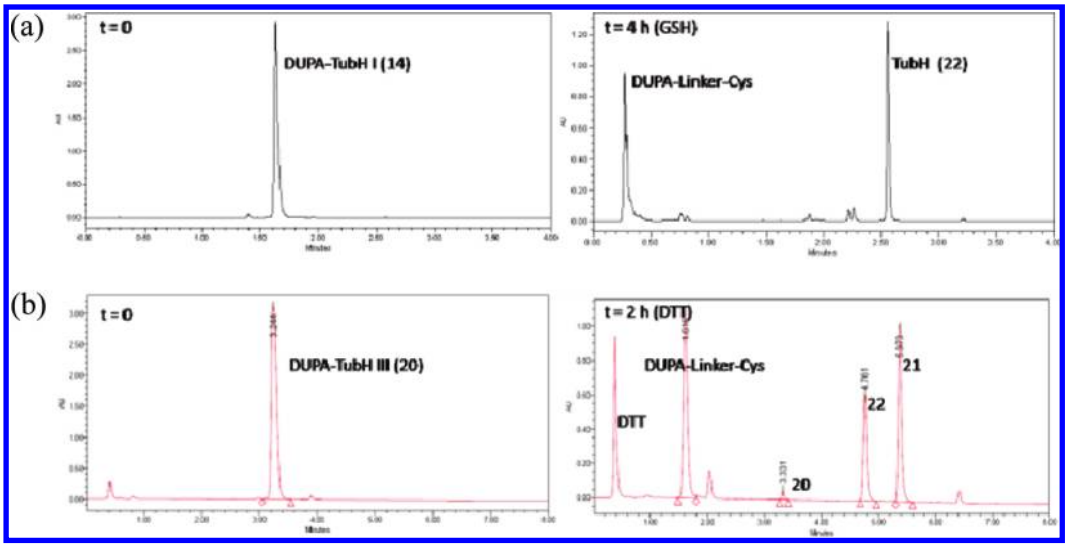

Figure 5. Release of TubH (**21**) from DUPA-TubH self-immolative prodrug (**14** or **20**) by disulfide reduction. DUPA-TubH was analyzed using (a) analytical RP-HPLC [A = 10 mM NH_4OAc (pH 7.0), and B = CH_3CN; λ = 257 nm: 10−100% B in 4 min] and (b) LC/MS [A = 10 mM NH_4OAc (pH 7.0), and B = CH_3CN; λ = 257 nm: 5−80% B in 8 min] in the absence (left chromatogram) and presence (right chromatogram) of a excess of (a) GSH or (b) DTT. See Scheme 4 for identities of products of the disulfide reduction reaction.

Scheme 4. Possible Mechanisms for Disulfide-Mediated Release of TubH from PSMA-Targeted Self-Immolative Prodrugs, Such as DUPA-TubH III, in the Presence of Disulfide Reducing Agents

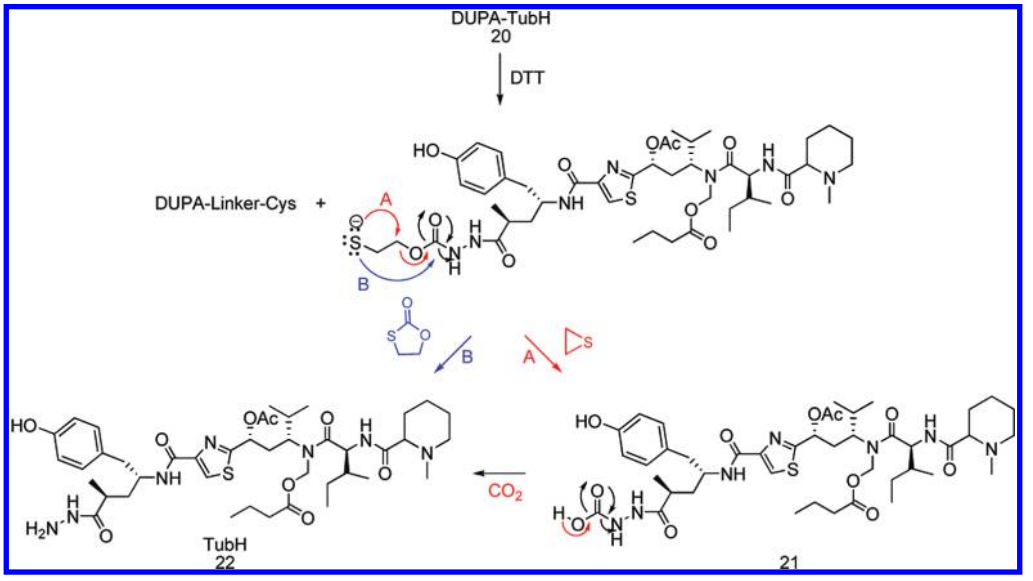

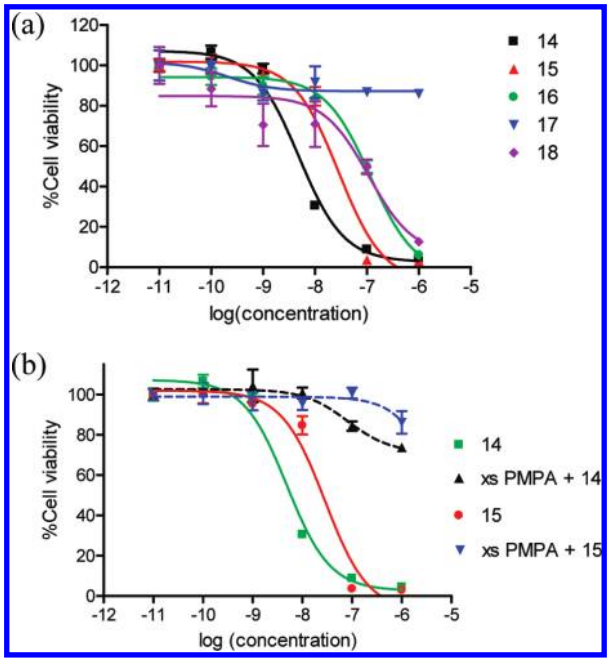

Figure 6. Effect of DUPA-targeted drug concentration on the survival of human PCa cells in the absence (a) and presence (b) of excess competitive inhibitor of PSMA (PMPA). DUPA-drug conjugates, dissolved in saline, were added at the indicated concentrations to LNCaP cells in RPMI culture media and allowed to incubate for 2 h at 37 °C. In competition experiments, 100-fold excess PMPA was added prior to DUPA conjugate addition to block all available PSMA sites on the LNCaP cells. Following 2 h of incubation, media were removed and replaced with fresh media (drug-free), and incubation was continued for an additional 66 h. Cell survival was then quantitated using a ^{3}H-thymidine assay, as described in the General Methods. Error bars represent SD ($n = 3$).

Table 2. Effect of Various DUPA-Targeted Cytotoxic Drugs on the Survival of LNCaP Cells in Culture

targeted drug	RF[a]	IC_{50} (nM)	clog P[b]
14	26	6 ± 2	3.38
15	25	31 ± 3	−2.26
16	7	115	−2.99
17	34	none[c]	−4.77
18	70	107	4.19
19	NA[d]	24	7.70
20	NA[d]	5 ± 2	3.60

[a] RF, relative affinity. [b] clog P = calculated log (partition coefficient). See the legend to Figure 2 for structures of DUPA-targeted drugs. [c] None, not active within the 100 pM to 1 μM range; SD (n = 2). [d] NA, not applicable.

mechanism must be designed that is inert during transit to the pathologic lesion but rapidly activated following target cell binding/internalization, leading to drug release at the site of disease.[12,37,38,41,43] Finally, for membrane impermeable drugs, an endosome escape strategy must also be designed that will ensure access of the released drug to the cytosol following uptake by the diseased cell. While much progress has been made in the development of these escape mechanisms, significant improvements will be necessary before the full potential of macromolecular drugs such as siRNAs, proteins, and nanoparticles can be realized.[45−48]

Acknowledgment. This work was supported by a grant from Endocyte, Inc.

Supporting Information Available: Structures of nontargeted cytotoxic drugs, copies of ^{1}H NMR spectra of all newly synthesized compounds, and HPLC profiles for targeted drug conjugates. This material is available free of charge via the Internet at http://pubs.acs.org.

References

(1) Van der Hul, R. L.; Seynaeve, C.; van Gell, B. N.; Verweij, J. Low dose of methotrexate and vinblastine, given weekly to patients with Desmoid tumors, is associated with major toxicity. *Sarcoma* **2003**, *7*, 153–157.
(2) Onyenadum, A.; Gogas, H.; Markopoulos, C.; Bafaloukos, D.; Aravantinos, G.; Mantzourani, M.; Koutras, A.; Tzorakoelefterakis, E.; Xiros, N.; Makatsoris, T.; Fountzilas, G.; Kalofonos, H. P. Mitoxantrone plus vinorelbine in pretreated patients with metastatic breast cancer. *J. Chemother.* **2007**, *19*, 582–589.
(3) Rahmani, R.; Zhou, X. J. Pharmacokinetics and metabolism of vinca alkaloids. *Cancer Surv.* **1993**, *17*, 269–281.
(4) Rowinsky, E. K.; Chaudhry, V.; Cornblath, D. R.; Donehower, R. C. Neurotoxicity of Taxol. *J. Natl. Cancer Inst. Monogr.* **1993**, *15*, 107–115.
(5) Rowinsky, E. K.; Eisenhauer, E. A.; Chaudhry, V.; Arbuck, S. G.; Donehower, R. C. Clinical toxicities encountered with paclitaxel (Taxol). *Semin. Oncol.* **1993**, *20*, 1–15.
(6) Ivachtchenko, A. V.; Kiselyov, A. S.; Tkachenko, S. E.; Ivanenkov, Y. A.; Balakin, K. V. Novel mitotic targets and their small-molecule inhibitors. *Curr. Cancer Drug Targets* **2007**, *7*, 766–784.
(7) Druker, B. J. Translation of the Philadelphia chromosome into therapy for CML. *Blood* **2008**, *112*, 4808–4817.
(8) Rabatti, D. The discovery of antiangiogenic molecules: a historical review. *Curr. Pharm. Des.* **2009**, *15*, 345–352.
(9) Li, W. W.; Hutnik, M.; Gehr, G. Antiangiogenesis in haematological malignancies. *Br. J. Hamaetol.* **2008**, *143*, 622–631.
(10) Mauro, M. J. Appropriate sequencing of tyrosine kinase inhibitors in chronic myelogenous leukemia: When to change? A perspective in 2009. *Curr. Opin. Hematol.* **2009**, *16*, 135–139.
(11) Breccia, M.; Frustaci, A. M.; Cannella, L.; Soverini, S.; Stefanizzi, C.; Federico, V.; Grammatico, S.; Santopietro, M.; Alimena, G. Sequential development of mutant clones in an imatinib resistant chronic myeloid leukaemia patient following sequential treatment with multiple tyrosine kinase inhibitors: An emerging problem? *Cancer Chemother. Pharmacol.* **2009**, *64*, 195–197.
(12) Ojima, I. Guided molecular missiles for tumor-targeting chemotherapy-case studies using the second-generation taxoids as warheads. *Acc. Chem. Res.* **2008**, *41*, 108–119.
(13) Balhorn, R.; Hok, S.; Burke, P. A.; Lightstone, F. C.; Cosman, M.; Zemla, A.; Mirick, G.; Perkins, J.; Natarajan, A.; Corzett, M.; DeNardo, S. J.; Albrecht, H.; Gregg, J. P.; DeNardo, G. L. Selective high-affinity ligand antibody mimics for cancer diagnosis and therapy: Initial application to lymphoma/leukemia. *Clin. Cancer Res.* **2007**, *15*, 5621s–5628s.
(14) Allen, T. M. Ligand-targeted therapeutics in anticancer therapy. *Nat. Rev. Cancer* **2002**, *2*, 750–763.
(15) Low, P. S.; Kularatne, S. A. Folate-targeted therapeutic and imaging agents for cancer. *Curr. Opin. Chem. Biol.* **2009**, *13*, 256–262.
(16) Larsen, A. K.; Escargueil, A. K.; Skladanowski, A. Resistance mechanisms associated with altered intracellular distribution of anticancer agents. *Pharmacol. Ther.* **2000**, *85*, 217–229.
(17) Isaken, K.; Jonsson, R.; Omdal, R. Anti-CD20 treatment in primary Sjögren's syndrome. *Scand. J. Immunol.* **2008**, *68*, 554–564.
(18) Gisselbrecht, C. Use of rituximab in diffuse large B-cell lymphoma in the salvage setting. *Br. J. Hamaetol.* **2008**, *143*, 607–621.
(19) Hall, P. C.; Cameron, D. A. Current perspective-trastuzumab. *Eur. J. Cancer* **2009**, *45*, 12–18.
(20) Jean, G. W.; Shah, S. R. Epiderm growth factor receptor monoclonal antibodies for the treatment of metastatic colorectal cancer. *Pharmacotherapy* **2008**, *28*, 742–754.
(21) Zwanziger, D.; Beck-Sickinger, A. G. Radiometal targeted tumor diagnosis and therapy with peptide hormones. *Curr. Pharm. Des.* **2008**, *14*, 2385–2400.
(22) Schally, A. V. New approaches to the therapy of various tumors based on peptide analogues. *Horm. Metab. Res.* **2008**, *40*, 315–322.
(23) Nishimura, Y.; Bereczky, B.; Ono, M. The EGFR inhibitor gefitinib suppresses ligand-stimulated endocytosis of EGFR via the early/late endocytic pathway in non-small cell lung cancer cell lines. *Histochem. Cell Biol.* **2007**, *127*, 541–553.
(24) Ye, X.; Yang, D. Recent advances in biological strategies for targeted drug delivery. *Cardiovasc. Hematol. Disord. Drug Targets* **2009**, *9*, 206–221.
(25) Yan, H.; Tram, K. Glycotargeting to improve cellular delivery efficiency of nucleic acids. *Glycoconjugate J.* **2007**, *24*, 107–123.

(26) Irache, J. M.; Salman, H. H.; Gamazo, C.; Espuelas, S. Mannose-targeted systems for the delivery of therapeutics. *Expert Opin. Drug Delivery* **2008**, *5*, 703–724.
(27) Corti, A.; Curnis, F.; Arap, W.; Pasqualini, R. The neovasculature homing motif NGR: More than meets the eye. *Blood* **2008**, *112*, 2628–2635.
(28) Gupta, Y.; Kohli, D. V.; Jain, S. K. Vitamin B12-mediated transport: A potential tool for tumor targeting of antineoplastic drugs and imaging agents. *Crit. Rev. Ther. Drug Carrier Syst.* **2008**, *25*, 347–379.
(29) Kularatne, S. A.; Wang, K.; Santhapuram, H. K.; Low, P. S. Prostate-specific membrane antigen targeted imaging and therapy of prostate cancer using a PSMA inhibitor as a homing ligand. *Mol. Pharmaceutics* **2009**, *6*, 780–789.
(30) Ghosh, A.; Heston, W. D. Tumor target prostate specific membrane antigen (PSMA) and its regulation in prostate cancer. *J. Cell Biochem.* **2004**, *91*, 528–539.
(31) Chang, S. S.; O'Keefe, D. S.; Bacich, D. J.; Reuter, V. E.; Heston, W. D.; Gaudin, P. B. Prostate-specific membrane antigen is produced in tumor-associated neovasculature. *Clin. Cancer Res.* **1999**, *5*, 2674–2681.
(32) Liu, H.; Rajasekaran, A. K.; Moy, P. Constitutive and antibody-induced internalization of prostate-specific membrane antigen. *Cancer Res.* **1998**, *58*, 4055–4060.
(33) Silver, D. A.; Pellicer, I.; Fair, W. R.; Heston, W. D.; Cordon-Cardo, C. Prostate-specific membrane antigen expression in normal and malignant human tissues. *Clin. Cancer Res.* **1997**, *3*, 81–85.
(34) Slusher, B. S.; Tsai, G.; Yoo, G.; Coyle, J. T. Immunocytochemical localization of the N-acetyl-aspartyl-glutamate (NAAG) hydrolyzing enzyme N-acetylated α-linked acidic dipeptidase (NAALADase). *J. Comp. Neurol.* **1992**, *315*, 217–229.
(35) Kularatne, S. A.; Zhou, Z.; Yang, J.; Post, C. B.; Low, P. S. Design, synthesis, and preclinical evaluation of prostate-specific membrane antigen targeted ^{99m}Tc-radioimaging agents. *Mol. Pharmaceutics* **2009**, *6*, 790–800.
(36) Vlahov, I. R.; Wang, Y.; Kleindl, P. J.; Leamon, C. P. Design and regioselective synthesis of a new generation of targeted chemotherapeutics. Part II: Folic acid conjugates of tubulysins and their hydrazides. *Bioorg. Med. Chem. Lett.* **2008**, *18*, 4558–4561.
(37) Vlahov, I. R.; Santhapuram, H. K.; Kleindl, P. J.; Howard, S. J.; Stanford, K. M.; Leamon, C. P. Design and regioselective synthesis of a new generation of targeted chemotherapeutics. Part 1: EC145, a folic acid conjugate of desacetylvinblastine monohydrazide. *Bioorg. Med. Chem. Lett.* **2006**, *16*, 5093–5096.
(38) Henne, W. A.; Doorneweerd, D. D.; Hilgenbrink, A. R.; Kularatne, S. A.; Low, P. S. Synthesis and activity of a folate peptide camptothecin prodrug. *Bioorg. Med. Chem. Lett.* **2006**, *16*, 5350–5355.
(39) Pessah, N.; Reznik, M.; Shamis, M.; Yantiri, F.; Xin, H.; Bowdish, K.; Shomron, N.; Ast, G.; Shabat, D. Bioactivation of carbamate-based 20(S)-camptothecin prodrugs. *Bioorg. Med. Chem.* **2004**, *12*, 1859–1866.
(40) de Groot, F. M.; Busscher, G. F.; Aben, R. W.; Scheeren, H. W. Novel 20-carbonate linked prodrugs of camptothecin and 9-amino-camptothecin designed for activation by tumour-associated plasmin. *Bioorg. Med. Chem. Lett.* **2002**, *12*, 2371–2376.
(41) Kratz, F.; Muller, I. A.; Ryppa, C.; Warnecke, A. Prodrug strategies in anticancer chemotherapy. *Chem. Med. Chem.* **2008**, *3*, 20–53.
(42) Sega, E. I.; Low, P. S. Tumor detection using folate receptor-targeted imaging agents. *Cancer Metastasis Rev.* **2008**, *27*, 655–664.
(43) Zhao, X.; Li, H.; Lee, R. J. Targeted drug delivery via folate receptor. *Expert Opin. Drug Delivery* **2008**, *5*, 309–319.
(44) Tarragó-trani, M. T.; Storrie, B. Alternative routes for drug delivery to the cell interior: Pathways to the Golgi apparatus and endoplasmic reticulum. *Adv. Drug Delivery Rev.* **2007**, *59*, 782–797.
(45) Whitehead, K. A.; Langer, R.; Anderson, D. G. Knocking down barriers: advances in siRNA delivery. *Nat. Rev. Drug Discovery* **2009**, *8*, 129–138.
(46) Aigner, A. Cellular delivery in vivo of siRNA-based therapeutics. *Curr. Pharm. Des.* **2008**, *14*, 3603–3619.
(47) Oh, Y. K.; Park, T. G. siRNA delivery systems for cancer treatment. *Adv. Drug Delivery Rev.* **2009**, *61*, 850–862.
(48) Walchli, S.; Sioud, M. Vector-based delivery of siRNAs: in vitro and in vivo challenges. *Front. Biosci.* **2008**, *13*, 3488–3493.